



CHORUS

This is the accepted manuscript made available via CHORUS. The article has been published as:

## Partition function zeros and phase transitions for a square-well polymer chain

Mark P. Taylor, Pyie Phyo Aung, and Wolfgang Paul  
Phys. Rev. E **88**, 012604 — Published 18 July 2013

DOI: [10.1103/PhysRevE.88.012604](https://doi.org/10.1103/PhysRevE.88.012604)

# Partition function zeros and phase transitions for a square-well polymer chain

Mark P. Taylor\* and Pyie Phyo Aung

*Department of Physics, Hiram College, Hiram, OH 44234, USA*

Wolfgang Paul

*Institut für Physik, Martin-Luther-Universität, D-06099 Halle (Saale), Germany*

## Abstract

The zeros of the canonical partition functions for flexible square-well polymer chains have been approximately computed for chains up to length 256 for a range of square-well diameters. We have previously shown that such chain molecules can undergo a coil-globule and globule-crystal transition as well as a direct coil-crystal transition. Here we show that each of these transitions has a well-defined signature in the complex-plane map of the partition function zeros. The freezing transitions are characterized by nearly circular rings of uniformly spaced roots, indicative of a discontinuous transition. The collapse transition is signaled by the appearance of an elliptical horse-shoe segment of roots that pinches down towards the positive real axis and defines a boundary to a root-free region of the complex plane. With increasing chain length, the root density on the circular ring and in the space adjacent to the elliptical boundary increases and the leading roots move towards the positive real axis. For finite length chains, transition temperatures can be obtained by locating the intersection of the ellipse and/or circle of roots with the positive real axis. A finite size scaling analysis is used to obtain transition temperatures in the long chain (thermodynamic) limit. The collapse transition is characterized by crossover and specific heat exponents of  $\phi \approx 0.76(2)$  and  $\alpha \approx 0.66(2)$ , respectively, consistent with a second order phase transition.

PACS numbers: 64.60.Bd, 64.60.an, 64.70.km

Keywords: partition function zeros, Yang-Lee theorem, Fisher zeros, square-well chain, finite size scaling

---

\* taylormp@hiram.edu

## I. INTRODUCTION

The study of partition function zeros has been an important topic in statistical physics since Yang and Lee proposed a general theory of phase transitions based on the behavior of the zeros of the grand canonical partition function in the complex fugacity plane [1, 2]. In the Yang-Lee theory, the non-analytic behavior of thermodynamic functions at phase transitions arises from the movement of some partition function zeros onto the positive real axis in the thermodynamic limit. Yang and Lee demonstrated this behavior for the Ising model in an external field. This approach was extended by Fisher who first studied the zeros of the canonical partition function (for the zero-field 2D Ising model) in the complex temperature plane [3]. The distribution and behavior of these Yang-Lee and Fisher zeros have been studied in a large number of systems and provide a means of computing phase transition properties including location, order, strength, and critical exponents [4–11]. In the thermodynamic limit the Yang-Lee zeros typically accumulate onto smooth curves in the complex fugacity plane while, in many cases (with the isotropic Ising model being an exception), the Fisher zeros densely cover well-defined areas in the complex temperature plane [12]. For a recent review of the partition function zero formalism and applications see Ref. [13]. Finally, although usually studied in the context of the thermodynamic limit, partition function zeros also provide a means of describing phase changes in finite size systems [14].

One application of the partition function zero method has been to study conformational phase transitions of model polymer chains. In particular, the approach has been used to study the collapse transition for lattice homopolymers [15–21], the protein-like folding transition of lattice heteropolymers [22, 23], and the helix-coil transition of a continuum polymer model [24, 25]. With the exception of Refs. [22] and [23], these polymer applications have focused on the scaling properties of the partition function zeros and attempted to obtain results for the long chain limit. These previous polymer studies have been restricted to rather modest chain lengths (typically  $N \leq 36$ ) and thus the partition function zero "maps" are relatively sparse.

In this work we study the partition function zeros for a continuum square-well-sphere polymer chain model. We have computed the density of states for this model system using the Wang-Landau simulation algorithm [26, 27] and, thus, can directly construct the canoni-

cal partition function. Using both canonical and microcanonical analyses we have previously demonstrated that this chain model exhibits interesting phase behavior for both finite chains and in the long chain limit [28, 29]. This model is also amenable to direct computation of the zeros of the canonical partition function since the latter is simply a polynomial whose coefficients are given by the density of states. Additionally, we are able to determine the partition functions for significantly longer chains than used in previous partition function zero studies of polymers. This allows us to more clearly establish relations between general features of the zero maps and single-chain phase transitions.

## II. MODEL AND METHODS

### A. Square-well chain model

In this work we study a single polymer chain comprised of  $N$  spherical monomers connected by “universal joints” of fixed bond length  $L$ . Monomer  $i$  is located by the position vector  $\vec{r}_i$  and all pairs of non-bonded sites  $i$  and  $j$  ( $|i - j| > 1$ ) interact via the square-well (SW) potential

$$u(r) = \begin{cases} \infty & r < \sigma \\ -\epsilon & \sigma < r < \lambda\sigma \\ 0 & r > \lambda\sigma \end{cases} \quad (1)$$

where  $r = r_{ij} = |\vec{r}_i - \vec{r}_j|$ ,  $\sigma$  is the hard-core diameter, and  $\epsilon$  and  $\lambda\sigma$  are the SW depth and width, respectively. In this work we set  $L = \sigma$  and use  $\epsilon$  to define the reduced temperature  $T^* = k_B T / \epsilon$ , where  $k_B$  is the Boltzmann constant. For a polymer at fixed temperature  $T$ , the single-chain canonical partition function is the Boltzmann weighted integral over all chain conformations and can be written as [30–32]

$$Z_N(T) = \int \cdots \int S_N \prod_{i < j+1}^N e^{-u(r_{ij})/k_B T} d\vec{r}_{12} \cdots d\vec{r}_{N-1,N} \quad (2)$$

where  $S_N = \prod_{i=1}^{N-1} \delta(r_{i,i+1} - L) / 4\pi L^2$  is the product of intramolecular distribution functions imposing the fixed bond length constraint and we have taken site 1 as the coordinate origin.

The SW-chain model has a discrete potential energy spectrum with allowed energy states  $E_n = -n\epsilon$  where  $n$  is the number of SW “overlaps” in a given chain conformation with

$0 \leq n \leq n_{max}$  and the  $N$ -dependent ground state energy is  $E_{gs} = -n_{max}\epsilon$ . The canonical partition function can be written as a sum over energy states as follows [31, 32]

$$Z_N(T) = \sum_{n=0}^{n_{max}} g(E_n) e^{-E_n/k_B T} = \sum_{n=0}^{n_{max}} g_n y^n \quad (3)$$

where  $g_n = g(E_n)$  is the density of states for energy level  $E_n$  and  $y = e^{1/T^*}$ .

## B. Partition function zeros and thermodynamics

As seen in Eq. (3), the SW chain canonical partition function can be expressed as a polynomial of order  $n_{max}$  in the temperature dependent variable  $y$ . This partition function can be rewritten in product form in terms of the  $n_{max}$  zeros or roots  $\{y_k\}$  of the polynomial as

$$Z_N(T) = \prod_{k=1}^{n_{max}} (y - y_k). \quad (4)$$

These polynomial zeros are generally complex, coming in symmetric pairs  $y_k = a_k \pm ib_k$  and, since the  $g_n$  are all positive, any real roots  $y_k = a_k$  are necessarily negative. All of the information contained in the polynomial coefficients  $\{g_n\}$  is contained in the polynomial roots  $\{y_k\}$ . Thus, all thermodynamic functions derivable from  $Z_N(T)$  can be expressed in terms of the partition function roots. For example, the single-chain specific heat can be written as

$$\begin{aligned} \frac{C(T)}{Nk_B} &= \frac{\beta^2}{N} \frac{\partial^2 \ln Z_N}{\partial \beta^2} = \frac{y(\ln y)^2}{N} \sum_{k=1}^{n_{max}} \frac{-y_k}{(y - y_k)^2} \\ &= \frac{y(\ln y)^2}{N} \sum_{k=1}^{n_{max}} \frac{(-a_k(y - a_k)^2 + b_k^2(2y - a_k))}{((y - a_k)^2 + b_k^2)^2} \end{aligned} \quad (5)$$

where  $\beta = 1/k_B T$  and here  $y$  is taken as a real number such that  $1 < y < \infty$  corresponds to the physical temperature range  $\infty > T^* > 0$ . The large  $y$  limit of Eq. (5) allows us to establish the additional property  $\sum_k a_k \leq 0$  for the  $Z(T)$  zeros since  $C(T)$  is a positive quantity. Notice that roots with small imaginary part  $b_k$  and positive real part  $a_k$  make a large contribution to  $C(T)$  near  $y = a_k$ . In general, roots closest the positive real axis, known as the leading roots, give the maximum contribution to thermodynamic quantities. As noted in the Introduction, the Yang-Lee theory of phase transitions is based on the convergence of these leading roots onto the positive real axis in the thermodynamic limit

(i.e.,  $N \rightarrow \infty$ ). For finite size systems, phase changes are typically identified from peaks in the specific heat [Eq. (5)] and thus, in principle, can also be located from the leading roots of the partition function.

### C. Simulation and numerical methods

We have previously carried out extensive simulation studies of the SW chain model [28, 29] using the Wang-Landau (WL) algorithm [26, 27] to construct the density of states function  $g(E)$ . In this approach, one generates a sequence of chain conformations using a set of Monte Carlo (MC) moves, however, rather than accepting moves according to a temperature dependent Boltzmann weight (i.e., via the Metropolis criterion), one uses the following temperature independent multicanonical probability

$$P_{acc}(a \rightarrow b) = \min \left( 1, \frac{w_{a \rightarrow b} g(E_a)}{w_{b \rightarrow a} g(E_b)} \right) \quad (6)$$

where  $w_{a \rightarrow b}$  and  $w_{b \rightarrow a}$  are weight factors which ensure microscopic reversibility for a given MC move type [33, 34]. In the WL approach  $g(E)$  is constructed in an iterative and dynamic fashion where smaller scale refinements are made at each level of the iteration. Successful implementation of this method requires an MC move set that is capable of efficiently exploring all configuration space. We use a combination of single bead crankshaft, reptation, and end-bridging moves and a multi-bead pivot move [34, 35]. The end-bridging move is found to be critical to exploring compact chain structures. We have tested the WL algorithm with our MC move set through comparison with exact  $g(E)$  data for short chains [32] and with MC results of Zhou et al. for longer chains [36]. As described in Ref. [29], in our implementation of the WL algorithm we carry out preliminary simulations to estimate the ground state energy of the chain and then set the minimum energy actually sampled in the WL simulation to be a few energy units above this ground state estimate. In the following,  $n_{max}$  refers to this minimum energy used in the WL simulation rather than to the true ground state energy level.

For long chains,  $n_{max}$  can be quite large (e.g., for  $N = 256$ ,  $n_{max} \gtrsim 1000$ ) and thus accurate numerical methods are required to compute the roots of the  $Z_N(T)$  polynomial [Eq. (3)]. For these calculations we have used MATHEMATICA [37]. To verify the sets of roots, we compute the specific heat function  $C(T)$  across the full temperature range using

Eq. (5) and compare with  $C(T)$  results computed directly from the original  $g(E)$  [28, 29]. In all cases we carry out three or more independent WL simulations and estimate uncertainties from the variations in resulting properties.

### III. RESULTS

#### A. Partition function zero maps

In Fig. 1 we show density of states functions, in the form  $\ln[g(E)/g(0)]$ , for SW chains with SW diameter  $\lambda = 1.10$  and chain lengths  $N = 32, 64, 128,$  and  $256$ . For these four chains lengths the canonical partition functions are given by polynomials of order 86, 200, 447, and 956, respectively, with the  $g(E)$  as the polynomial coefficients. In the case of  $N = 256$  these coefficients span approximately 680 orders of magnitude. One can reduce the large range covered by the polynomial coefficients through the rescaling

$$Z_N(T) = \sum_{n=0}^{n_{max}} c_n (y/A)^n \quad (7)$$

with  $c_n = A^n g_n$ . For example, in the case of  $N = 256, \lambda = 1.10$ , a choice of  $A = 10$  will give scaled coefficients that span approximately 275 (rather than 680) orders of magnitude. We find, however, that MATHEMATICA yields exactly equivalent results with or without such a rescaling of the  $Z_N(T)$  polynomials.

The zeros of the  $Z_N(T)$  polynomials, obtained from the Fig. 1 density of state functions, are shown in the complex  $y$ -plane in Fig. 2. The number of zeros in each case corresponds to the above noted polynomial order. These “root maps” are exactly symmetric with respect to the  $\text{Re}(y)$ -axis and the mean of the real parts  $a_k = \text{Re}(y_k)$  of the roots is negative as expected. Specific heat functions computed via Eq. (5) with these sets of roots are shown in Fig. 3 and are found to be identical to the specific heat functions computed directly from the density of states as done in Refs. [28, 29]. (As an aside, the low temperature  $C(T)$  shoulder seen in Fig. 3 for  $N = 32$  is primarily due to the large negative real root omitted from the Fig. 2a root map).

The root maps shown in Fig. 2 exhibit remarkable structure that becomes more defined with increasing chain length. In particular, there is an outer circle of roots that becomes denser and smaller in diameter for the long chains. The distribution of roots on this circle

is approximately uniform, including in the vicinity of the  $\text{Re}(y)$ -axis where the leading roots close in on the axis with increasing  $N$ . Such a uniform root density is characteristic of a first order transition [9]. Inside this circle is an elliptical horseshoe boundary with a fan-like tail that demarcates a root free region of the complex plane. The junction of the horseshoe and fan corresponds to a second set of leading roots that pinch down closer to the  $\text{Re}(y)$ -axis with increasing  $N$ . This behavior appears to follow the Yang-Lee model for phase transitions with roots approaching the positive real axis with increasing system size and, in the thermodynamic limit, dividing the real axis into single phase regions separated by phase transitions. In Fig. 2 physical temperatures lie on the positive real axis and are given by  $T^* = 1/\ln(y)$ . Thus, we expect the leading roots on the circular ring to correspond to a low temperature transition while the leading roots on the elliptical horseshoe correspond to a higher temperature transition. More specifically, we associate the circle of roots with chain freezing and the elliptical boundary with chain collapse. Although the root maps obtained from our multiple independent WL simulations can show significant variation in the location of some individual roots, these circular and elliptical boundaries, and in particular the leading roots, are highly reproducible. This is shown in Fig. 4 where we plot three sets of roots obtained from three independent WL simulations for  $N = 128$ ,  $\lambda = 1.10$ . Note that the single set of roots shown in each part of Fig. 2 is computed using the average of the density of states from multiple simulations.

## B. Finite chain transition temperatures

One typically uses the partition function zeros to obtain information about phase transitions in the thermodynamic limit [7]. Thus, as will be described in Sec. III-D, transition temperatures and critical exponents are obtained by studying the approach of the leading zeros towards the positive real axis [8, 9]. In a finite size system the location of the leading zeros can also provide some information on the location and nature of changes in state of the system [14]. Describing such state changes in finite size systems is of relevance to polymers, and in particular biopolymers, where a thermodynamic (i.e., infinite chain length) limit is never really achieved. As noted in the Introduction, although there has also been some use of partition function zeros to study conformational transitions of finite length chains [22, 23], most previous studies involving polymers have focussed on scaling behavior and the

TABLE I. Transition temperatures obtained from the canonical specific heat (SH) [Fig. 3] and from the partition function zero maps (ZM) [Fig. 5] for SW chains with length  $N$  and SW diameter  $\lambda = 1.10$ . The numbers in parentheses are uncertainty estimates in the last digits shown.

$N$	$T_f^*(\text{SH})$	$T_f^*(\text{ZM})$	$T_c^*(\text{SH})$	$T_c^*(\text{ZM})$
32	0.370(1)	0.370(1)	0.492(1)	0.500(6)
64	0.450(1)	0.450(1)	0.537(1)	0.535(9)
128	0.515(1)	0.515(1)	0.576(1)	0.578(4)
256	0.563(2)	0.564(1)	0.603(3)	0.601(3)

long chain limit [15–17, 19–21, 24, 25]. In this section we focus on the conformational phase transitions of finite length SW chain.

As noted above, the freezing transition of the SW chain is clearly associated with the circular ring of roots observed in the Fig. 2 root maps and extrapolation to the positive real axis is straightforward. By fitting the leading pair of roots to a circle of radius  $R^2 = a_k^2 + b_k^2$  we find that the intersection point with the positive real axis  $y_f = R$  gives freezing transition temperatures  $T_f^* = 1/\ln y_f$  in agreement with those previously obtained from the canonical specific heat functions. We show examples of these fits to the leading roots on the freezing circle for  $\lambda = 1.10$  in Fig. 5a and give numerical results in Table 1. The uncertainty estimates included in Table 1 reflect the variation in results obtained from our multiple WL simulations for each case. With increasing  $N$ , the root density on the circle increases and the intersection point becomes very close to the real part of the leading root. This circle fitting procedure must be done locally as the large circle of roots is often slightly perturbed near the positive real axis protruding out in the positive direction. Thus  $R$  given above is not always identical to the average radius of the full circle seen in the root maps. We note that in the canonical ensemble calculations, the freezing transition temperatures were taken from the rather sharp specific heat maxima shown in Fig. 3. Of course, these peaks do have a nonzero width, reflective of the fact that for finite  $N$  the transition must be gradual.

The collapse transition of the SW chain is associated with the pinching down of the elliptical horse-shoe boundary and fan-shaped tail towards the real positive axis. The two lines of roots, defining the left and right sides of this pinch-down region, are non-orthogonal to the  $\text{Re}(y)$ -axis which is consistent with a continuous phase transition [4–6]. Similarly,

the asymmetry of the left and right sides of the pinch-down region is consistent with an asymmetric specific heat peak at the collapse transition (as observed in Fig. 3). This asymmetry in the root boundary also suggests that the location of the leading root,  $y_1$ , alone will not be sufficient to estimate the transition point for a finite length chain. Here we propose a geometric construction that uses the entire set of roots defining the elliptical boundary, including the cluster of roots in the immediate neighborhood of the leading root at the pinch-down point, to locate the finite-chain transition point. We fit this set of boundary points  $\{a_k, b_k\}$  to an ellipse  $((a-c)/r_a)^2 + (b/r_b)^2 = 1$  [38], as shown in Fig. 5b, and take the intersection of the fit ellipse with the real positive axis at  $y_c = r_a + c$  to locate the collapse transition temperature  $T_c^* = 1/\ln y_c$ . This approach appears to be quite reliable for longer chains where we find quantitative agreement with previous results for the  $N = 128$  and 256 chains (see Table I). For the shorter  $N = 32$  and 64 chains this construction is somewhat less robust since the points defining the boundary are fewer in number and less well defined than for the long chains.

The fact that the effective transition temperatures obtained for finite  $N$  from the specific heat and the circle and ellipse fits of the partition function zeros close to the  $\text{Re}(y)$ -axis are in such good agreement is founded on the fact that the major contribution to the specific heat peaks comes from these sets of zeros as previously noted and evident in Eq. (5). If one would analyze other physical properties of the finite polymer chains, slightly different effective transition temperatures might be expected. Such behavior is general for finite size scaling of phase transitions, where peaks of specific heat, susceptibility, temperature derivative of the average absolute value of the magnetization, etc., all are known to differ for finite  $N$ , although they converge to the same critical temperature in the limit of  $N \rightarrow \infty$  [39].

One notable feature of the phase behavior of the SW chain model is the disappearance of the collapse transition for a sufficiently short range SW-interaction [28]. For the case of chain length  $N = 128$  we have previously demonstrated, using a microcanonical thermodynamic analysis, that a collapsed globule phase is not stable for  $\lambda \leq 1.05$  [29]. This same conclusion can be reached, in a somewhat more direct fashion, using the above described partition function zero approach for locating phase changes in finite size systems. In Fig. 6 we show the evolution of the partition function root maps for the  $N = 128$  SW chain with increasing SW diameter  $\lambda$ . These roots maps include an ellipse fit to the set of roots defining the

TABLE II. Transition temperatures obtained from canonical and microcanonical specific heat functions (SH) (Ref. [29]) and from the partition function zero maps (ZM) [Figs. 6 and 8] for SW chains with length  $N = 128$  and SW diameter  $\lambda$ . The numbers in parentheses are uncertainty estimates in the last digits shown.

$\lambda$	$T_f^*(\text{SH})$	$T_f^*(\text{ZM})$	$T_c^*(\text{SH})$	$T_c^*(\text{ZM})$
1.02	0.363(2)	0.363(2)	- - - -	0.321(22)
1.05	0.446(1)	0.446(1)	0.426(2)	0.422(5)
1.06	0.465(1)	0.465(1)	0.463(4)	0.458(4)
1.07	0.481(2)	0.481(1)	0.495(3)	0.488(4)
1.08	0.495(2)	0.495(1)	0.516(2)	0.514(6)
1.15	0.526(2)	0.526(1)	0.714(2)	0.705(5)
1.25	0.342(6)	0.345(3)	1.010(5)	0.996(6)
1.30	- - - -	- - - -	1.165(5)	1.151(5)

elliptical horseshoe boundary. For  $\lambda > 1.06$  this ellipse intersects the positive real axis to the left of the freezing circle in which case  $T_{\text{collapse}} > T_{\text{freezing}}$ , and thus, a stable collapsed globule phase exists in the intervening temperature region. However, for cases with  $\lambda < 1.06$  we observe that the ellipse crosses the freezing circle, intersecting the positive real axis to the right of this circle. This corresponds to  $T_{\text{collapse}} < T_{\text{freezing}}$  which implies that chain collapse is preempted by the freezing transition and no stable globule phase exists. The globule may still occur as a metastable state and, since its free energy difference from the stable state is finite, it may still contribute to some extent to thermal averages. This idea is supported by the close proximity of the intersection of the circle and ellipse fits with the  $\text{Re}(y)$ -axis in the case of  $\lambda = 1.05$ . For the case of  $\lambda = 1.06$  we see the intersection points of the ellipse and the freezing circle with the positive real axis nearly coincide, locating the triple point (or tricritical endpoint expected for  $N \rightarrow \infty$ ) in the SW chain  $T^*$  vs  $\lambda$  phase diagram (Fig. 6 in Ref. [29]). In Table II we compare transition temperatures obtained from the ellipse and circle fits to the root map boundary points with results previously obtained from analysis of both microcanonical and canonical specific heat functions [29]. These numerical results are in exact agreement for the freezing transition and in very close agreement for the collapse transition.

### C. On the origin of the circle

A particularly intriguing feature of the partition function zero maps for the SW chain model is the nearly perfect circle of roots associated with the freezing transition. This circular pattern calls to mind the original work of Lee and Yang on the Ising model [2] and their famous circle theorem proving that the complex roots of the Ising grand partition function all lie on the unit circle. In particular, Lee and Yang demonstrated that real polynomials of the form  $P(y) = c_0 + c_1y + c_2y^2 + \dots + c_{n-1}y^{n-1} + y^n$  with coefficients  $c_k$  given by sums of products of all  $i, j$ -bipartite partitionings of the real numbers  $a_{ij} = a_{ji}$  ( $i \neq j, 1 \leq i, j \leq n$ ) with magnitudes  $|a_{ij}| \leq 1$ , have roots confined to the unit circle. The coefficients of the Lee-Yang polynomial possess the mirror symmetry  $c_k = c_{n-k}$  and thus these polynomials are a special case of the general class of self-reciprocal polynomials defined by the relation  $P(y) = y^n P(1/y)$ . Although the SW chain partition function is not of this Lee-Yang form, the region of the partition function associated with chain freezing can be approximately written as a self-reciprocal polynomial  $P(y)$ , with positive coefficients  $c_k \leq 1$  where  $c_k > c_{k+1}$  for  $k \leq n/2$ . Such self-reciprocal polynomials with decreasing positive coefficients also have their zeros confined to the unit circle [40, 41] and, thus, we have an approximate local “circle theorem” for the SW chain freezing transition. The local self-reciprocal behavior of the SW chain partition function is revealed by making a rescaling transformation of the type shown in Eq. (7).

To both demonstrate and understand the origin of a local Lee-Yang type symmetry in the coefficients of the SW chain  $Z_N(T)$  polynomial it is useful to consider the microcanonical analysis of a discontinuous phase transition [42]. In the microcanonical approach, curvature properties of the entropy function  $S(E) = k_B \ln g(E)$  are used to define types of phase transitions in finite size systems. A discontinuous or first-order transition is identified by the presence of a convex intruder in  $S(E)$ . Both the energy range spanned by the transition and the transition temperature can be determined from a double tangent line construction across the convex intruder (where the tangent points define the energy range and the slope gives the inverse of the transition temperature). The double tangent construction is shown in Fig. 7a for a SW chain with  $N = 128$  and  $\lambda = 1.10$ . In general, this double tangent line is

given by  $-n/T_f^* + b$  and can be used to transform the partition function to a new polynomial

$$Z_N(T) = e^b \sum_{n=0}^{n_{max}} c_n (y/y_f)^n \quad (8)$$

with coefficients  $c_n = e^{n/T_f^* - b} g_n$  and where  $y_f = e^{1/T_f^*}$ . The transformed coefficients for the  $N = 128$ ,  $\lambda = 1.10$  SW chain (for which  $T_f^* = 0.5151$  and  $b = 98.95$ ) are shown in Fig. 7b. In the region of the first order transition ( $214 \leq n \leq 375$ ) the  $c_n$  coefficients are seen to possess at least an approximate version of the Lee-Yang mirror symmetry. The zeros of this part of the polynomial, corresponding to the freezing transition, are found to lie almost exactly on the unit circle as shown in the inset in Fig. 7a. Furthermore, the circle of roots obtained from only this limited part of the  $Z_N(T)$  polynomial almost exactly coincides with the corresponding roots from the full polynomial shown in Fig. 2c (noting the scale factor of  $y_f$  relating the two root maps). We note that an exact mirror symmetry between the coefficients across the freezing transition would not be expected for the present problem due to the lack of symmetry between the two states that coexist at the transition (unlike the Ising model with its exact symmetry with respect to inversion of all spins together with inversion of the magnetic field).

In our previous study of the phase behavior of the  $N = 128$  SW chain [29] we noted the weakening of the freezing transition with increasing square well diameter  $\lambda$  and the disappearance of a convex intruder in  $S(E)$  for  $1.22 \leq \lambda \leq 1.45$ . Given the direct connection we have established between the convex intruder and the circular ring of zeros, we expect the absence of a convex intruder to imply the absence of a circle in the associated root map. In Fig. 8 we show this is the case, as the root maps for  $\lambda = 1.25$  and  $1.30$  lack the well-defined circle feature. However, for the case of  $\lambda = 1.25$  [Fig. 8a] there is a pair of leading roots approaching the  $Re(y)$ -axis which can be associated with a sparse circle of roots. This sparse circle arises from a small energy range ( $460 \lesssim n \lesssim 470$ ) where  $S(E)$  is nearly linear (but never convex), as evidenced by a strong local flattening of  $dS(E)/dE$  in this region. Our geometric construction for the freezing transition temperature yields  $T_f^* = 0.345(3)$ , in agreement with our previous analysis based on the location of specific heat peaks. In the case of  $\lambda = 1.30$  [Fig. 8c] there is no evidence in the root map for a freezing transition. Numerical results for collapse transition temperatures, obtained by fitting ellipses to the root boundaries seen in Figs. 8b and 8d, are given in Table II.

## D. Scaling Analysis

In the original theory of Yang and Lee [1] the non-analytic behavior of thermodynamic functions at phase transitions arises from the movement of a set of partition function zeros (the leading zeros) onto the positive real axis as the thermodynamic limit is taken. By studying the approach of these leading roots towards the positive real axis as a function of system size one can estimate both transition temperatures and scaling exponents characterizing the infinite size system [43]. For the polymer collapse transition this finite size scaling is governed by the crossover exponent  $\phi$  [44–46] which measures the distance of closest approach for the finite size system to the  $N \rightarrow \infty$  transition point. Thus, the distance between the leading partition function zero and the true transition point  $y_c$  is expected to scale as [19, 21, 24, 43]

$$y_1(N) - y_c \sim DN^{-\phi} \quad (9)$$

where  $D = d_1 + id_2$  is a complex constant. (For a magnetic or fluid system the polymer exponent  $\phi$  would be replaced by  $1/d\nu$ , where  $d$  is dimensionality and  $\nu$  is the correlation length exponent). Given that  $y_c$  is unknown, and that the imaginary part of the leading root vanishes in the thermodynamic limit, the standard scaling analysis extracts the exponent  $\phi$  from the scaling of the imaginary part alone through the relation [19, 21, 24]

$$\text{Im}[y_1(N)] \sim d_2 N^{-\phi}. \quad (10)$$

In Fig. 9a we show scaling plots of the imaginary part of leading roots at the elliptical pinch-down point (associated with the collapse transition) versus chain length  $N$  for chains with square-well diameters in the range  $1.05 \leq \lambda \leq 1.30$ . The lines are power law fits for each  $\lambda$  and the resulting crossover exponents  $\phi$  are given in Table III. Although these crossover exponents vary somewhat with  $\lambda$ , they are all consistent with a value of  $\phi \approx 0.76(2)$ .

We use these  $\phi$  results to determine the collapse transition temperature in the  $N \rightarrow \infty$  limit by studying the leading roots in the complex inverse temperature plane defined by:  $\ln(y_k) = \beta_k + i\tau_k$  where  $\beta_k = \ln(a_k^2 + b_k^2)^{1/2}$  and  $\tau_k = \tan^{-1}|b_k/a_k|$ . The real part of this leading root is expected to scale as [24, 47]

$$\beta_1(N) \sim \beta_c + (d_1/y_c)N^{-\phi} \quad (11)$$

where  $\beta_c = 1/T_c^*$  gives the transition point. In Fig. 9b we show plots of  $\beta_1(N)$  vs  $N^{-\phi}$  using the  $\phi$  values given in Table III. The lines are linear fits for each  $\lambda$  data set and the resulting

TABLE III. Finite size scaling results from the leading partition function zeros for SW chains with SW diameter  $\lambda$ . For the collapse transition we include the crossover exponent  $\phi$ , the inverse transition temperature  $\beta_c$ , the specific heat exponents  $\alpha\phi$  and  $\alpha$ , the exponent relation  $2 - \alpha - 1/\phi$ , and the transition temperature  $T_c^*$ . For the freezing transition we give the  $N \rightarrow \infty$  transition temperature  $T_f^*$ . The numbers in parentheses are uncertainty estimates in the last digits shown.

$\lambda$	$\phi$	$\beta_c$	$\alpha\phi$	$\alpha$	$2 - \alpha - 1/\phi$	$T_c^*$	$T_f^*$
1.05	0.762(8)	2.194(10)	0.496(2)	0.651(7)	0.037(21)	0.456(2)	0.616(2)
1.10	0.727(8)	1.548(5)	0.457(2)	0.629(7)	-0.005(22)	0.646(2)	0.758(1)
1.15	0.759(11)	1.222(6)	0.502(7)	0.661(13)	0.021(32)	0.818(4)	0.853(3)
1.18	0.745(16)	1.071(10)	0.482(2)	0.647(14)	0.011(43)	0.934(9)	0.936(16)
1.20	0.764(6)	0.992(6)	0.505(5)	0.660(8)	0.031(18)	1.008(6)	0.897(15)
1.25	0.783(7)	0.836(4)	0.539(5)	0.688(9)	0.035(20)	1.196(6)	0.540(7)
1.30	0.770(11)	0.709(7)	0.530(2)	0.688(10)	0.013(28)	1.410(14)	- - - -

$\beta_c$  (and  $T_c^*$ ) values are given in Table III. An alternate method to finding the transition temperature, which does not explicitly use the exponent  $\phi$ , is to plot the leading roots in the form  $\text{Im}[y_1(N)]$  vs  $\beta_1(N)$ . The scaling assumptions given in Eqs. (10) and (11) imply that these roots will fall on a straight line that intercepts the  $\beta$ -axis at the transition point  $\beta_c$ . Our results from this construction (not shown) are in agreement with those obtained from the original method, supporting the consistency of the Eq. (10) and (11) scaling forms.

Given the  $N \rightarrow \infty$  collapse transition temperature  $T_c$  we can carry out a finite size scaling analysis of the specific heat [Eq. (5)] which is expected to exhibit the following behavior

$$C(T_c)/Nk_B \sim |T - T_c|^{-\alpha} \sim N^{\alpha\phi}. \quad (12)$$

In Fig. 9c we show a scaling plot of the specific heat at the  $N \rightarrow \infty$  collapse transition temperature  $T_c^*$  versus chain length  $N$ . The lines are power law fits for each  $\lambda$  data set and the resulting exponents  $\alpha\phi$  and  $\alpha$  are given in Table III. The exponent  $\alpha$  shows some variation with well diameter  $\lambda$  but our results are all consistent with a value of  $\alpha \approx 0.66(2)$  for the range  $1.05 \leq \lambda \leq 1.30$ .

The self-consistency of the exponents  $\alpha$  and  $\phi$  can be checked by noting that, for large  $N$ , Eq. (5) gives  $C(T_c)/Nk_B \sim 1/Nb_1^2$  where  $b_1 = \text{Im}(y_1)$ . Combining this with Eq. (10) gives

$C(T_c)/Nk_B \sim N^{2\phi-1}$  which, upon comparison with Eq. (12) gives the exponent identity  $2 - \alpha = 1/\phi$  [45]. As shown in Table III, this identity is satisfied, or nearly satisfied, for the cases studied here with our mean values giving  $\alpha + 1/\phi = 1.98(4)$ . As expected, both  $\phi < 1$  and  $\alpha < 1$  supporting the idea that the collapse transition is, in the thermodynamic limit, a true second order phase transition [47].

In the case of the freezing transition we expect finite size effects to be dominated by the relatively large fraction of sites forming the surface of the frozen chain. In this situation the transition temperature for a chain of length  $N$  will be shifted from the infinite chain value by a term proportional to the surface-to-volume ratio of the frozen chain. This gives the scaling behavior [48]

$$T_f(N) \sim T_f(\infty) - BN^{-1/3} \quad (13)$$

where the finite chain transition temperature is given directly by the leading root associated with freezing in the complex temperature plane as  $T_f^*(N) = 1/\beta_1(N)$ . In Fig. 10 we show plots of  $T_f^*(N)$  versus  $N^{-1/3}$  for SW diameters in the range  $1.05 \leq \lambda \leq 1.25$ . The lines are linear fits for each  $\lambda$  data set and the resulting  $T_f^*(\infty)$  values are given in Table III. Comparison of the  $N \rightarrow \infty$  collapse and freezing transition temperatures show that  $T_c < T_f$  for  $\lambda < 1.18$  and thus, for these small SW diameters, chain collapse is pre-empted by the freezing transition giving a direct coil→crystal transition. We have shown this behavior previously for finite length chains [28, 29], but here we see that it persists in the long chain limit with a coil-globule-crystal triple point existing for SW diameter  $\lambda \approx 1.18$ .

In the above scaling analysis for the collapse transition we have used an approach that would be appropriate to study a normal critical point. However, the collapse transition is generally thought to be a tricritical point with upper critical dimension three [49]. This implies that in three dimensions the collapse transition should exhibit mean-field behavior ( $\phi = 1/2$ ,  $\alpha = 0$ ) with logarithmic corrections. The predicted tricritical scaling behavior is [50]

$$\text{Im}[y_1(N)] \sim N^{-1/2}(\ln N)^{-\mu} \quad (14)$$

and

$$C(T_c)/Nk_B \sim (\ln N)^\zeta \quad (15)$$

where the logarithmic correction exponents are given by  $\mu = 7/11$  and  $\zeta = 3/11$ . Verifying this scaling behavior using simulation data has proven difficult as very long chains are

required to clearly establish the logarithmic correction terms [44, 46, 50, 51]. Fits of our data using the Eq. (14) and (15) scaling forms (not shown), give slightly larger  $\chi^2$  values than the fits to Eqs. (10) and (12) (shown in Fig. 9) and yield logarithmic correction exponents of  $\mu \approx 1.0(1)$  and  $\zeta \approx 2.2(2)$  which do not agree with the tricritical predictions.

#### IV. DISCUSSION

In this work we have studied the zeros of the canonical partition function for an isolated SW-chain polymer. The SW-chain is a continuum (i.e., non-lattice) model, but is characterized by a discrete energy spectrum and thus the partition function is simply given by a polynomial of order  $n_{max} = |E_{gs}/\epsilon|$  in the variable  $y = e^{1/T^*}$ . The partition function zeros encode the same information as the partition function itself, but the distribution of these zeros across the complex  $y$ -plane provides an alternate approach to identifying and characterizing phase transitions. The partition function zero or root maps for the SW-chain develop very clear patterns with increasing chain length that serve as signatures for different types of single chain conformational transitions. Here we have connected a circle of nearly uniformly spaced roots with the freezing transition (i.e., either the globule-crystallite or direct coil-crystallite transitions) and an elliptical horseshoe shaped boundary with the chain collapse transition. For finite length chains the leading roots on the circle are sufficient to determine a freezing transition temperature while an ellipse fit to the set of elliptical boundary points approximately locates the collapse transition temperature. The elliptical boundary connects with a fan-like tail at the point of closest approach to the  $\text{Re}(y)$ -axis. We associate this change in boundary geometry at the leading roots for the collapse transition with the different thermal behavior of the collapse transition when approached from above and from below (as seen in Fig. 3).

We have also established an approximate local “circle theorem” associated with the presence of a convex intruder in the microcanonical entropy function  $S(E)$ . In particular, a transformation of the partition function relative to the double tangent line spanning the convex intruder (and thus defining the transition region of width  $|\Delta E|$ ) produces a local self-reciprocal or mirror symmetry in the partition function polynomial coefficients. This self-reciprocal or Lee-Yang structure leads to a nearly uniform circle of exactly  $|\Delta E|/\epsilon$  zeros in the complex plane. Furthermore, it is found that the portion of the partition function for

energy states above the convex intruder (i.e., coil and globule states) produces zeros which are all inside the circle while the portion of the partition function for energy states below the convex intruder produces zeros which are all outside the circle. Thus, this circle exactly divides the complex plane into two regions corresponding to crystallite and non-crystallite states. Chomaz and Gulminelli have previously demonstrated a one-to-one correspondence between a bimodal probability distribution and the Lee-Yang theorem in the thermodynamic limit [11]. The connection we have drawn between the presence of a convex intruder in  $S(E)$  and Lee-Yang behavior is quite similar as the convex intruder generates a bimodal probability distribution.

The partition function zero maps we have presented for the SW chain model are not dissimilar from the root maps found for other chain models [15–19, 21, 23]. However, as noted in the Introduction, these previous studies have been restricted to rather modest length chains and, thus, the root maps typically resemble our results for  $N = 32$  shown in Fig. 2a. Short chains simply do not possess enough partition function zeros to display the well-defined structures we obtain for long chains. This problem is exacerbated in the case of lattice chains in two-dimensions as studied in most of the above cited references. The one chain molecule root map in the literature that has a different global topology for the ones presented here is that for an atomistic model of polyalanine computed by Alves and Hansmann [24]. This model has a continuous energy spectrum, which these authors discretized for the analysis of partition function zeros. The resulting zeros cover a disk region in the complex  $y$ -plane centered on the origin and within this disk is a dense circular ring of zeros. This disk region of roots is bisected by a root-free strip that runs along the full  $\text{Re}(y)$ -axis so the circular ring is actually two disconnected semicircles. This chain molecule undergoes a helix-coil transition and a scaling analysis of the leading roots for  $10 \leq N \leq 40$  found exponents  $\phi = 1.08(6)$  and  $\alpha = 0.86(10)$ , consistent with either a “strongly” second order or a “weakly” first order transition.

We have carried out a similar scaling analysis of the leading partition function zeros for SW chains with  $32 \leq N \leq 256$  which allows us to determine both transition temperatures and critical exponents in the  $N \rightarrow \infty$  limit. In this long chain limit the freezing and collapse transition temperatures are found to coincide for the case of  $\lambda \approx 1.18$ . For smaller SW diameters we find the collapse temperature to be *lower* than the freezing temperature, indicating that the collapse transition is preempted by the freezing transition. We have previously

shown this result for finite length chains [28, 29] but here we are able to demonstrate that a direct coil-crystal transition occurs in the long-chain limit. For the collapse (coil-globule) transition our scaling analysis gives a polymer crossover exponent of  $\phi \approx 0.76(2)$  and a specific heat exponent of  $\alpha \approx 0.66(2)$  for square-well diameters in the range  $1.05 \leq \lambda \leq 1.30$ . These exponents are consistent with a second-order phase transition in the thermodynamic limit [47]. Fitting our collapse data to a tricritical scaling theory (mean-field exponents with logarithmic corrections) gives correction terms not consistent with the predictions of tricritical scaling [50]. Although the recent work of Lee et al. [21] for very short chains ( $N \leq 24$ ) on a cubic lattice does report agreement with the Eq. (14) tricritical scaling form, the previous work of Meirovitch and Lim [44] on longer chains ( $N \leq 250$ ) find results similar to those reported here.

## ACKNOWLEDGMENTS

MPT thanks Jutta Luettmmer-Strathmann for helpful conversations and Kurt Binder for numerous stimulating discussions and insightful comments on this manuscript. Financial support from Hiram College, the National Science Foundation (DMR-0804370 and DMR-1204747), and the Deutsche Forschungsgemeinschaft (SFB TRR 102/A7 and SFB 625/A3) are gratefully acknowledged.

## REFERENCES

- [1] C. N. Yang and T. D. Lee, Phys. Rev. **87**, 404 (1952).
- [2] T. D. Lee and C. N. Yang, Phys. Rev. **87**, 410 (1952).
- [3] M. E. Fisher, in *Lectures in Theoretical Physics. Vol. 7C - Statistical Physics, Weak Interactions, Field Theory*, edited by W. E. Brittin (University of Colorado Press, Boulder, 1965) Chap. 1.
- [4] S. Grossmann and W. Rosenhauer, Z. Phys. **207**, 138 (1967).
- [5] S. Grossmann and W. Rosenhauer, Z. Phys. **218**, 437 (1969).
- [6] S. Grossmann and V. Lehmann, Z. Phys. **218**, 449 (1969).
- [7] S. Grossmann, Adv. Solid State Phys. **9**, 207 (1969).
- [8] G. Bhanot, R. Salvador, S. Black, P. Carter, and R. Toral, Phys. Rev. Lett. **59**, 803 (1987).
- [9] R. J. Creswick and S.-Y. Kim, Phys. Rev. E **56**, 2418 (1997).
- [10] W. Janke and R. Kenna, J. Stat. Phys. **102**, 1211 (2001).
- [11] P. Chomaz and F. Gulminelli, Physica A **330**, 451 (2003).
- [12] W. van Saarloos and D. A. Kurtze, J. Phys. A: Math. Gen. **17**, 1301 (1984).
- [13] I. Bena, M. Droz, and A. Lipowski, Int. J. Mod. Phys. B **19**, 4269 (2005).
- [14] P. Borrmann, O. Mulken, and J. Harting, Phys. Rev. Lett. **84**, 3511 (2000).
- [15] R. Finsky, M. Janssens, and A. Bellemans, J. Phys. A: Math. Gen. **8**, L106 (1975).
- [16] D. C. Rapaport, J. Phys. A: Math. Gen. **10**, 637 (1977).
- [17] V. Privman and D. A. Kurtze, Macromolecules **19**, 2377 (1986).
- [18] J. Lee, J. Korean Phys. Soc. **44**, 617 (2004).
- [19] J. H. Lee, S.-Y. Kim, and J. Lee, J. Chem. Phys. **133**, 114106 (2010).
- [20] J. H. Lee, S.-Y. Kim, and J. Lee, J. Chem. Phys. **135**, 204102 (2011).
- [21] J. H. Lee, S.-Y. Kim, and J. Lee, Phys. Rev E **86**, 011802 (2012).
- [22] J. Wang and W. Wang, J. Chem. Phys. **118**, 2952 (2003).
- [23] C.-N. Chen and C.-Y. Lin, Physica A **350**, 45 (2005).
- [24] N. A. Alves and U. H. E. Hansmann, Phys. Rev. Lett. **84**, 1836 (2000).
- [25] N. A. Alves and U. H. E. Hansmann, Physica A **292**, 2001 (2001).
- [26] F. Wang and D. P. Landau, Phys. Rev. Lett. **86**, 2050 (2001).
- [27] F. Wang and D. P. Landau, Phys. Rev. E **64**, 056101 (2001).

- [28] M. P. Taylor, W. Paul, and K. Binder, *Phys. Rev. E* **79**, 050801(R) (2009).
- [29] M. P. Taylor, W. Paul, and K. Binder, *J. Chem. Phys.* **131**, 114907 (2009).
- [30] M. P. Taylor, *J. Chem. Phys.* **114**, 6472 (2001).
- [31] M. P. Taylor, *Mol. Phys.* **86**, 73 (1995).
- [32] M. P. Taylor, *J. Chem. Phys.* **118**, 883 (2003).
- [33] F. A. Escobedo and J. J. de Pablo, *J. Chem. Phys.* **102**, 2636 (1995).
- [34] D. Reith and P. Virnau, *Comp. Phys. Comm.* **181**, 800 (2010).
- [35] D. P. Landau and K. Binder, *Monte Carlo Simulations in Statistical Physics* (Cambridge University, Cambridge, 2000).
- [36] Y. Zhou, M. Karplus, J. M. Wichert, and C. K. Hall, *J. Chem. Phys.* **107**, 10691 (1997).
- [37] Wolfram Research, Inc., *Mathematica, Version 8.0* (Wolfram Research, Inc., Champaign, Illinois, 2010).
- [38] A. Fitzgibbon, M. Pilu, and R. B. Fisher, *IEEE Trans. on Pattern Analysis and Machine Intelligence* **21**, 476 (1999).
- [39] A. M. Ferrenberg and D. P. Landau, *Phys. Rev. B* **44**, 5081 (1991).
- [40] W. Chen, *J. Math. Anal. Appl.* **190**, 714 (1995).
- [41] K. Chinen, *Discrete Math.* **308**, 6426 (2008).
- [42] D. H. E. Gross, *Microcanonical Thermodynamics* (World Scientific, Singapore, 2001).
- [43] C. Itzykson, R. B. Pearson, and J. B. Zuber, *Nucl. Phys. B* **220**, 415 (1983).
- [44] H. Meirovitch and H. A. Lim, *J. Chem. Phys.* **92**, 5144 (1990).
- [45] R. Brak, A. L. Owczarek, and T. Prellberg, *J. Phys. A* **26**, 4565 (1993).
- [46] T. Prellberg and A. L. Owczarek, *Phys. Rev. E* **51**, 2142 (1995).
- [47] M. Fugugita, H. Mino, M. Okawa, and A. Ukawa, *J. Stat. Phys.* **59**, 1397 (1990).
- [48] C. Borgs and R. Kotecky, *J. Stat. Phys.* **79**, 43 (1995).
- [49] P.-G. de Gennes, *Scaling Concepts in Polymer Physics* (Cornell University Press, Ithaca, 1979).
- [50] P. Grassberger and R. Hegger, *J. Chem. Phys.* **102**, 6881 (1995).
- [51] T. Vogel, M. Bachmann, and W. Janke, *Phys. Rev. E* **76**, 061803 (2007).

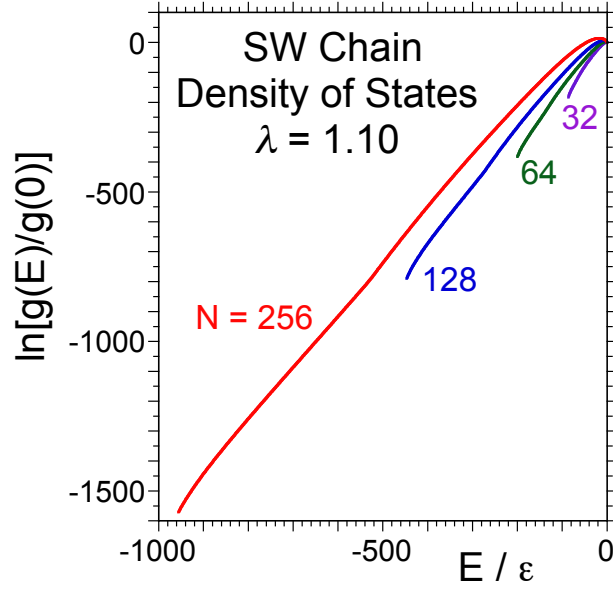


FIG. 1. (Color online) Logarithm of the density of states  $\ln g(E)$ , relative to the value at  $E = 0$ , vs energy  $E$  for a SW chain with SW diameter  $\lambda = 1.10$  and length  $N = 32, 64, 128$ , and  $256$ , as indicated.

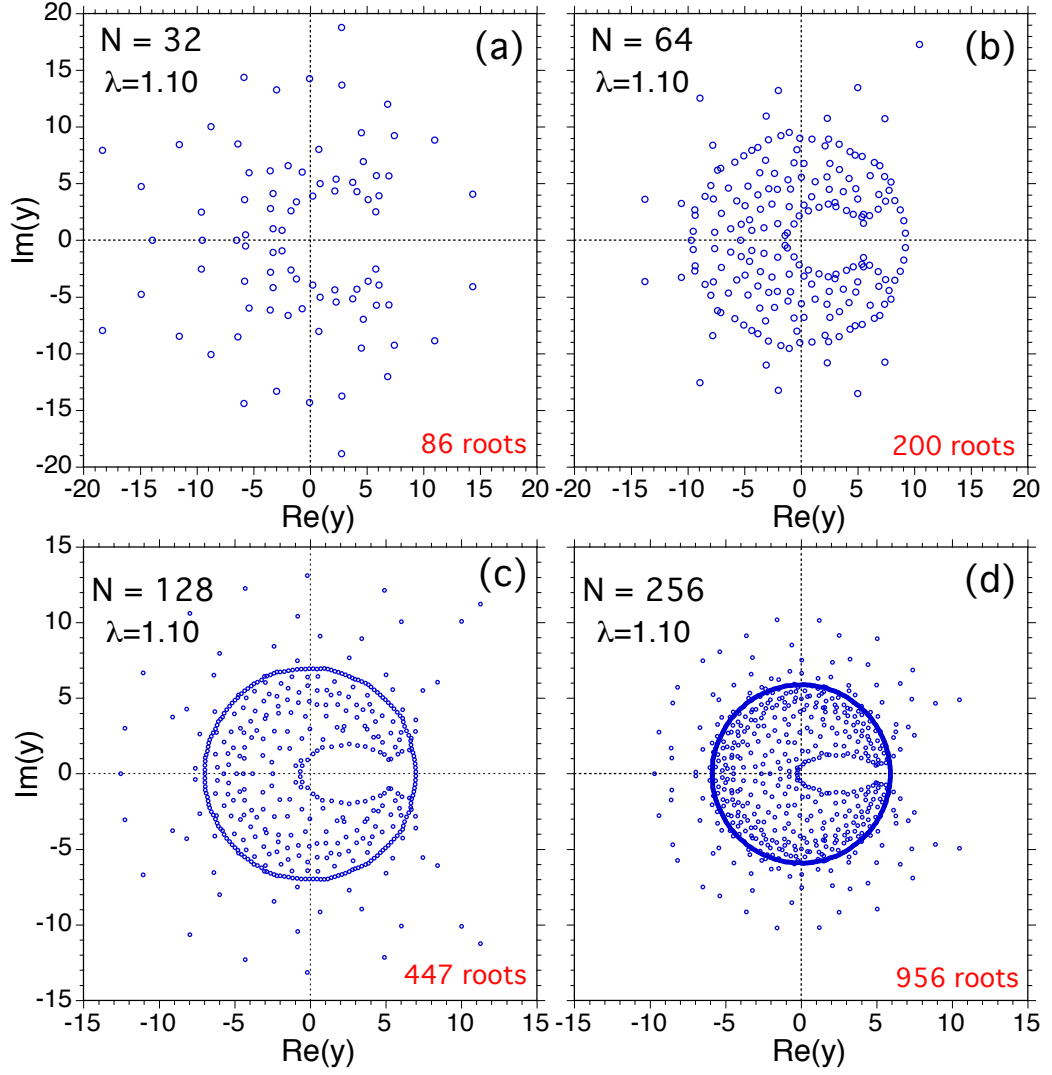


FIG. 2. (Color online) Partition function zeros in the complex  $y$ -plane for a SW chain with SW diameter  $\lambda = 1.10$  and length  $N =$  (a) 32, (b) 64, (c) 128, and (d) 256. Here  $y = e^{1/T^*}$  and positive physical temperatures correspond to the real axis with  $\text{Re}(y) > 1$ . The  $g(E)$  shown in Fig. 1 are the coefficients for the  $Z_N(T)$  polynomials whose roots are shown here. The number of roots in each case corresponds to the minimum energy used in the Wang-Landau sampling. In (a), one root located at  $y = -538 + 0i$  falls outside the plot range.

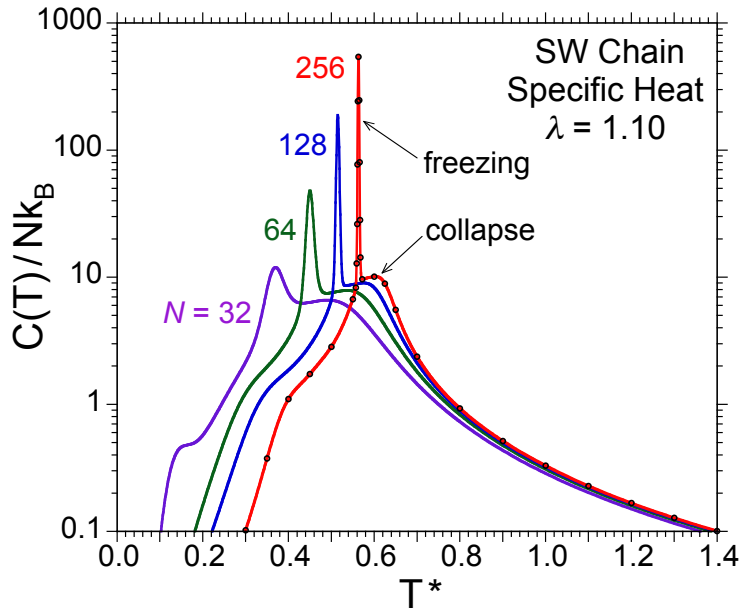


FIG. 3. (Color online) Specific heat per monomer  $C(T)/Nk_B$  vs temperature  $T^*$  for a SW chain with SW diameter  $\lambda = 1.10$  and length  $N = 32, 64, 128,$  and  $256$ , as indicated. These functions have been computed directly from the partition function zeros shown in Fig. 2 via Eq. (5). Chain collapse and freezing transitions are associated with the primary peaks in these functions. For  $N = 256$  we include, as symbols, results computed from the density states (which are found to be identical to results obtained from the partition function zeros).

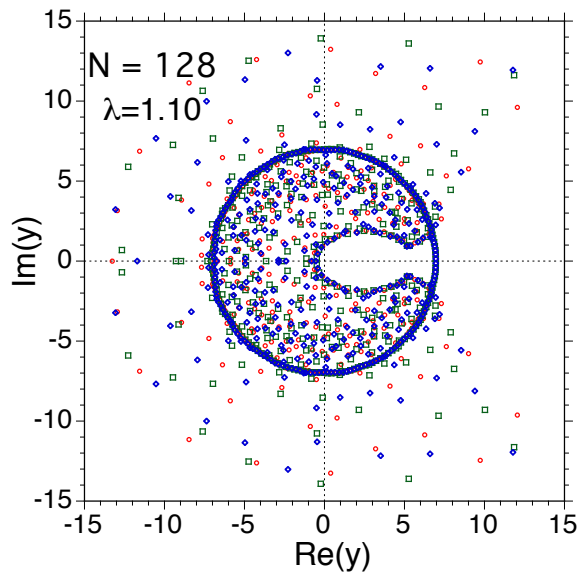


FIG. 4. (Color online) Partition function zeros in the complex  $y$ -plane for a SW chain with SW diameter  $\lambda = 1.10$  and length  $N = 128$ . Three sets of roots, obtained from three independent WL simulations, are plotted using a different symbol and color for each set. Notice that while individual roots can show significant variation, the elliptical and circular boundaries, and in particular, the leading roots are well reproduced.

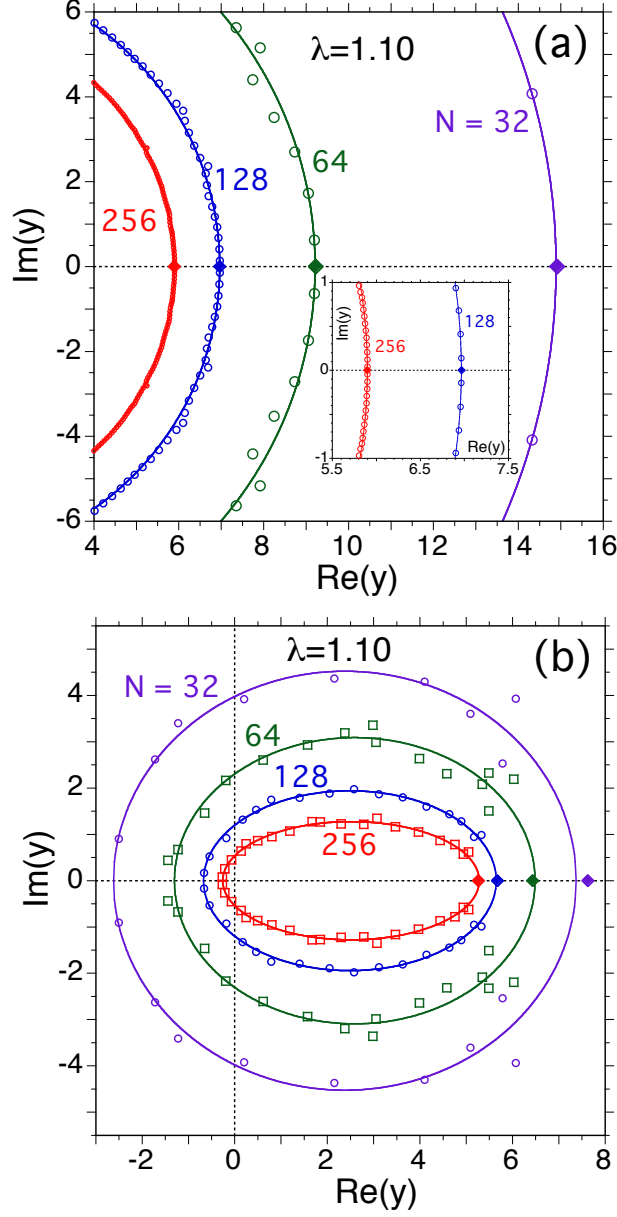


FIG. 5. (Color online) Partition function zeros forming (a) the circular ring and (b) the elliptical horseshoe boundary in the complex  $y$ -plane for a SW chain with SW diameter  $\lambda = 1.10$  and length  $N = 32, 64, 128$ , and  $256$ , as indicated. In (a) the solid lines are circles centered on the origin which pass through the leading pair of roots. In (b) the solid lines are fits to an ellipse for each set of data points shown. In (a) and (b) the filled symbols on the positive real axis correspond to the freezing and collapse transition temperatures, respectively, obtained from the specific heat curves shown in Fig. 3. The inset in (a) shows an expanded view of the  $N = 128$  and  $256$  roots near the positive  $\text{Re}(y)$ -axis.

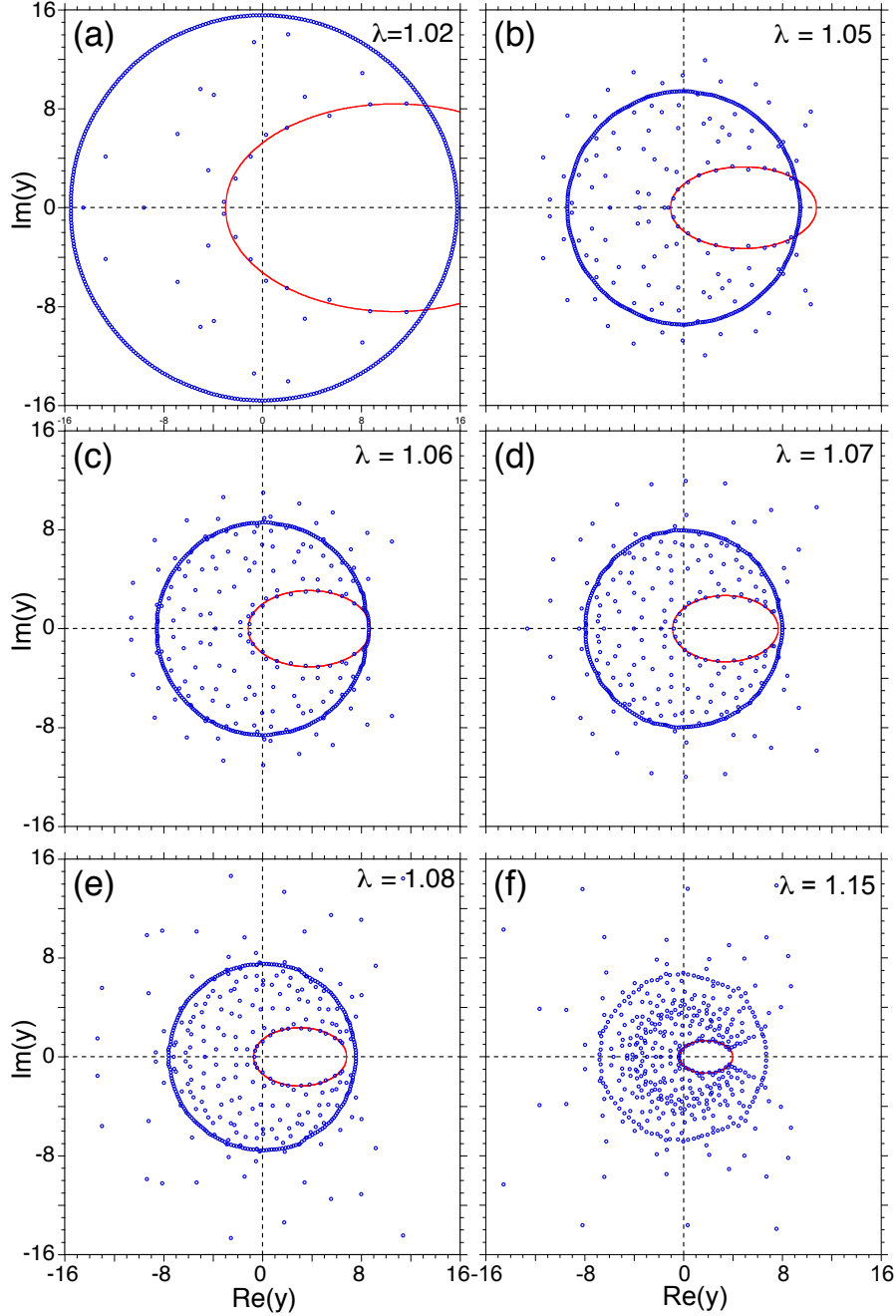


FIG. 6. (Color online) Partition function zeros in the complex  $y$ -plane for a SW chain with  $N = 128$  and square-well diameter  $\lambda$  of (a) 1.02, (b) 1.05, (c) 1.06, (d) 1.07, (e) 1.08, and (f) 1.15. In each case the solid line is an ellipse fit to the set of points defining the elliptical horseshoe boundary. The number of roots in each case corresponds to the minimum energy used in the Wang-Landau sampling and here range from 439 for (a) to 450 for (f) (see Ref. [29]). In (f) three pairs of roots fall outside the plot range.

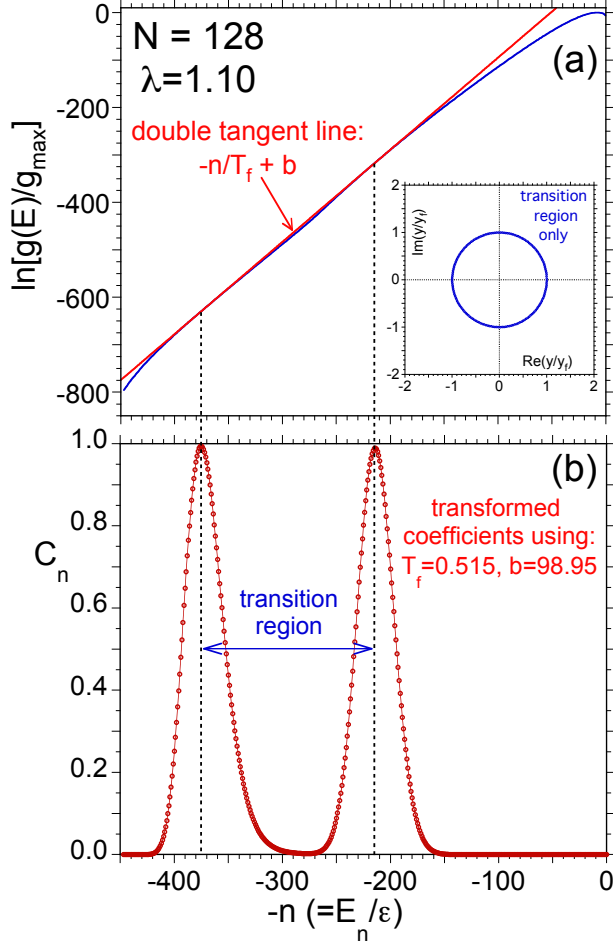


FIG. 7. (Color online) (a) Logarithm of the density of states  $\ln g(E)$  vs energy  $E$  for a SW chain with  $N = 128$  and  $\lambda = 1.10$ . The upper straight line is a double tangent construction used to identify the energy range associated with the first-order freezing transition. Inset: Zeros of the polynomial built from the transformed coefficients in the transition energy range. (b) Transformed coefficients  $c_n$  for the  $Z_N(T)$  polynomial in  $y/y_f$ . These coefficients are seen to possess an approximate mirror symmetry of the Lee-Yang type across the transition energy range.

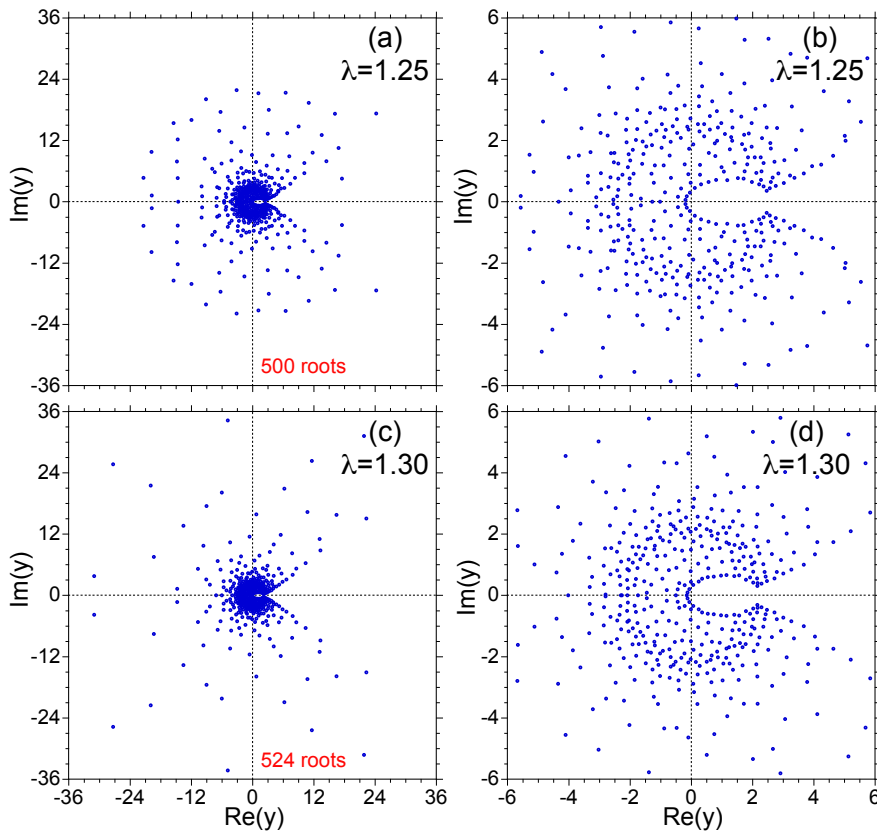


FIG. 8. (Color online) Partition function zeros in the complex  $y$ -plane for a SW chain with  $N = 128$  and SW diameter  $\lambda$  of (a,b) 1.25 and (c,d) 1.30. (b) and (d) provide expanded views of the elliptical boundary region associated with the collapse transition. In (a) there is a pair of leading roots approaching the  $\text{Re}(y)$ -axis at radial distance  $R = 18.1$  that is associated with a sparse circle of roots and a weak freezing transition. In (c) 19 roots fall outside the plot range, but none of these are near the positive real axis.

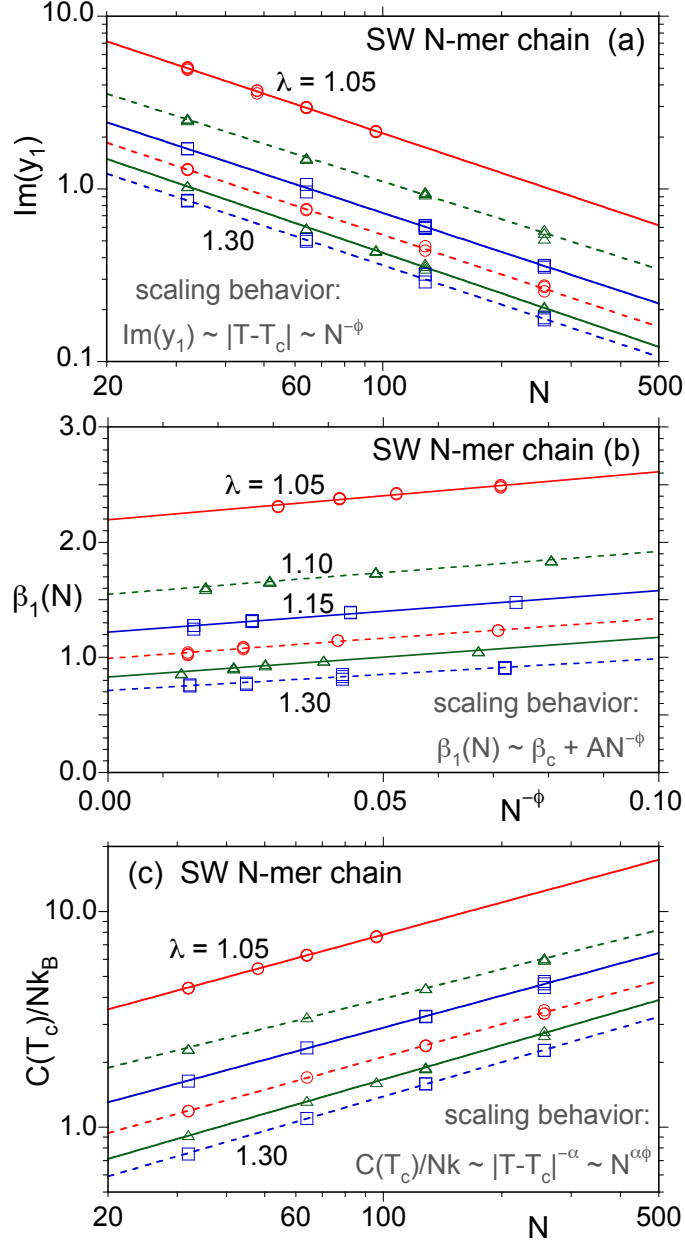


FIG. 9. (Color online) Scaling plots for the leading partition function zeros and specific heat for the collapse transition. In each case we show simulation results as symbols for SW diameters, from top to bottom, of  $\lambda = 1.05, 1.10, 1.15, 1.20, 1.25,$  and  $1.30$ . We include multiple results for each root obtained from independent WL simulations and the symbol sizes are larger than or comparable to the variation in these duplicate values. (a) The imaginary part of the leading roots  $y_1$  vs chain length  $N$  with power law fits shown as lines. (b) The real part of the leading complex temperature zero  $\beta_1$  vs scaled chain length  $N^{-\phi}$  where the exponents  $\phi$  for each  $\lambda$  are given in Table III and the lines are linear fits. (c) Specific heat  $C/Nk_B$  at the  $N \rightarrow \infty$  transition temperatures  $T_c$ , given in Table III, vs chain length  $N$  with power law fits shown as lines.

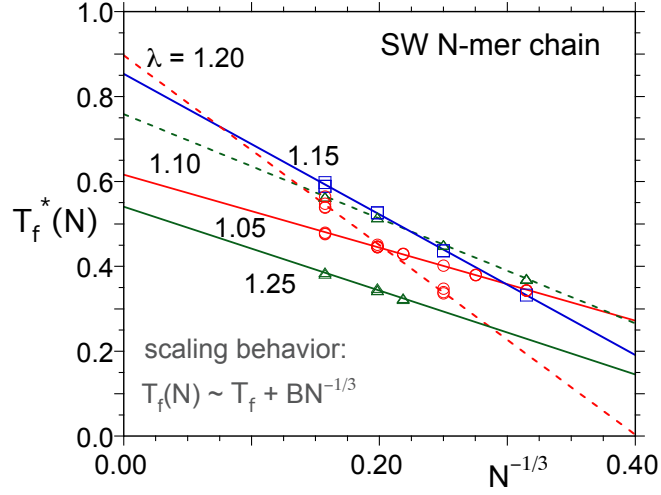


FIG. 10. (Color online) Finite size scaling plot for the freezing temperature  $T_f^*(N)$  of an  $N$ -mer SW chain vs scaled chain length  $N^{-1/3}$  for SW diameters in the range  $1.05 \leq \lambda \leq 1.25$ , as indicated. We include multiple results for each  $N$ ,  $\lambda$  combination, obtained from independent WL simulations, and the symbol sizes are larger than or comparable to the variation in these duplicate values. The lines are power law fits to each data set.